



Study on Crack Evolution Mechanism of Roadside Backfill Body in Gob-Side Entry Retaining Based on UDEC Trigon Model

Bowen Wu^{1,2} · Xiangyu Wang¹ · Jianbiao Bai² · Wenda Wu^{1,2} · Xiangxiang Zhu^{1,2} · Guodong Li^{1,2}

Received: 25 March 2018 / Accepted: 31 January 2019 / Published online: 21 March 2019
© Springer-Verlag GmbH Austria, part of Springer Nature 2019

Abstract

Gob-side entry retaining is a non-chain pillar mining technology in which reasonable roadside support is important for efficient roadway maintenance and goaf isolation in coal mines. A UDEC Trigon model is adopted in this paper to study the mechanism of crack expansion and evolution at various distances from the working face. This is done to optimize parameters for the roadside backfill body (RBB) by combining emergence, development and aggregation of micro-cracks with macroscopic mechanical responses. Results of the model show that cracks first appear in the top and bottom corner of the roadway in the lane-side RBB. Damage to the RBB is mainly caused by tensile cracks, which can be divided into main and secondary crack-development and yield-bearing zones. A reasonable aspect ratio of the RBB can greatly increase the area of the yield-bearing zone and reduce the damage degree, while reducing the number of penetrating cracks and preventing generation of seepage channels. The application of this model for gob-side entry retaining in the intake airway of the N2105 working face in the Yuwu coal mine indicates that deformation of the surrounding rocks can be effectively controlled.

Keywords Gob-side entry · Roadside backfill body · UDEC Trigon model · Crack development · Goaf isolation

1 Introduction

Gob-side entry retaining (GER) technique has recently become widely used in Chinese coal mines (Tan et al. 2015; Khaldoun et al. 2016). A GER structure is a type of roadway without pillars in which the former entry roadway is retained for transportation (or as a return air gate road) during mining of the next panel. This is achieved by constructing an artificial wall along the gob side in such a way that it lags behind the coal face being excavated (Ning et al. 2017). Compared with other longwall roadway layouts, GER has some advantages in terms of higher resource recovery rate and lower drivage ratio, and it solves the problem of gas concentration in the upper corner (Chen 2012a). With the application and development of high strength bolt support technology in coal mine, the deformation of roadways in the surrounding could be effectively controlled through laneway support. Thus, the

key part of GER technology is effective roadside support (Bi 2014). The reasonable design of roadside backfill bodies (RBBs) can control the deformation of surrounding rocks, improve the stress state of the surrounding rock and prevent harmful gas flowing into the roadway from the goaf (Chen et al. 2012b) (Fig. 1).

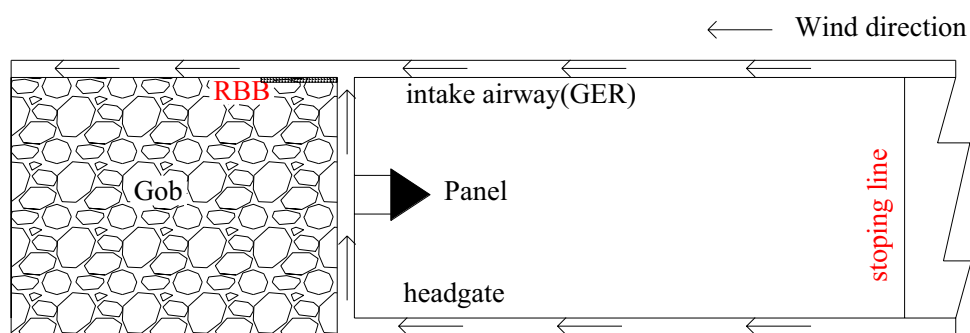
Most previous research into roadside support has focused on the RBB from a macroscopic perspective (Zhang et al. 2003; Kan et al. 2011). Ma et al. (2007) developed a mechanical model of the surrounding rock for entry-in packing in fully mechanized top-coal caving mining face and studied the interaction relationship between the packing body and the surrounding rock. The results show that the packing body and the surrounding rock can form a good and corporate load-carrying system. This can improve the bearing capacity of the surrounding rock, so the necessary packing body supporting resistance can be greatly reduced. Li et al. (2012) provided a formula for calculating the gob-side supporting resistance so as to determine a rational width of roadside backfill by building a mechanical model of key blocks and immediate roof and analyzing the interaction mechanism between key blocks and the surrounding rock around the gob-side entry retaining. However, macroscopic mechanical properties are the comprehensive manifestation

✉ Xiangyu Wang
wangxiangyu_cumt@163.com

¹ School of Mines, China University of Mining and Technology, Xuzhou 221116, China

² State Key Laboratory of Coal Resources and Safe Mining, Xuzhou 221116, China

Fig. 1 Sketch map of the GER showing the positions of the gob and RBB



of microscopic damage evolution (Guo 2017). In field applications, numerous joints and cracks can be generated in the RBB due to mining pressure, complex geotechnical conditions and the quality of backfilling, leading to reduction of RBB strength and loss of RBB's load-bearing capacity (Xu et al. 2018). Therefore, effective control of crack development in RBB can ensure the effect of gob-side entry retaining. Li et al. (2016) used the UDEC Voronoi model to study the influence of the location of key blocks on the development of cracks in the RBB. Li et al. (2017) established the UDEC model with Trigon logic to analyze the crack location of the lower rock in GER under different support conditions and its influence on the stability of the surrounding rock masses on the roadway. Hao (2017) used UDEC to study the influence of reinforcement parameters on the bearing capacity of the RBB. The results indicates that parameters of the reinforcement system can improve the lateral restraint ability against cracking, change the damage characteristics of the backfill and improve its bearing capacity.

UDEC is one of the mainstream softwares for studying the development of rock mass fissures. It fully considers the discontinuity of rock masses. The two basic components of the rock mass (the rock itself and structural planes) are described based on the principles of continuous mechanics

and contact, respectively (Lisjak and Grasselli 2014; Itasca Consulting Group Inc. 2011). The UDEC Trigon model used in this paper divides the hexagonal mesh into triangles based on Voronoi division. This effectively improves the calculation rate and makes the crack propagation process more consistent with experimental results (Itasca Consulting Group Inc. 2014). Compared with another simulation software FLAC (finite difference code), UDEC can effectively simulate the macroscopic mechanical responses and visually display the internal force behavior of the media based on full consideration of discontinuity in the rock mass. Originally, we used FLAC simulation method to design the aspect ratio of the RBB in the intake airway of the N2105 working face at Yuwu coal mine. The design aspect ratio was 1:2.4, and the "bulging" phenomenon appeared in the RBB during the mining process (Fig. 2), and the RBB was even destroyed in some severely damaged areas.

Previous research mainly focused on the support resistance, characteristics of deformation, mechanism of activity of the RBB or the distribution of crack in RBB under different crack locations of key block and support parameters. Few studies have focused on the crack evolution mechanism in RBB. In this paper, a UDEC Trigon model is adopted to analyze the mechanism of crack evolution of the RBB based



Fig. 2 "Bulging" deformation phenomenon occurs in the RBB

on the N2105 working face of the Yuwu coal mine of Shanxi Lu'an Mining Industry Group. Also, the influence of different aspect ratios on the stability of the roadway is studied based on micro-crack development in the RBB and analysis of macroscopic mechanical response.

2 Introduction of the UDEC Trigon Model

2.1 Fundamentals of the UDEC Trigon Model

Discrete cracks forming in the intact rock cannot be simulated in the initial version of UDEC, because the newly generated discontinuities cannot be driven by successive sections. This shortcoming was resolved by the proposal of polygonal block patterns by Lorig and Cundall (1989). Christianson (2006) and Alzo'ubi et al. (2009) verified the rationality of the polygonal block pattern by studying the rock failure mechanism with a Voronoi UDEC model. This was done by cutting all conventional UDEC Voronoi polygonal blocks into several constituent triangular blocks (Gao et al. 2014a), allowing the proposed UDEC Trigon model to be built. A rock is represented by an assembly of triangular blocks bonded together via their grain contacts. Each block is made elastic by dividing them into triangular finite difference zones. Hence, the block does not fail by plastic yielding. Failure can only occur along the contacts in shear or tension, depending on the stress state and the properties of the contact surface (Itasca Consulting Group Inc. 2014). In the direction perpendicular to a contact surface, the stress–displacement relation is assumed to be linear and determined by the stiffness (k_n), as given in Eq. (1):

$$\Delta\sigma_n = -k_n\Delta u_n, \tag{1}$$

where $\Delta\sigma_n$ is the effective normal stress increment and Δu_n is the normal displacement increment. A limiting tensile strength (T) is assumed for the contact. If this value is exceeded, then σ_n equals to 0.

In the direction parallel to a contact surface, the response is governed by a constant shear stiffness. The shear stress, τ_s , is

determined by contact properties, including cohesive (c) and frictional (φ). Where:

$$|\tau_s| \leq c + \sigma_n \tan \varphi = \tau_{\max}, \tag{2}$$

then

$$\Delta\tau_s = -k_s\Delta u_s^e. \tag{3}$$

However, if $|\tau_s| \geq \tau_{\max}$, then:

$$\tau_s = \text{sign}(\Delta u_s^e)\tau_{\max}, \tag{4}$$

where Δu_s^e is the elastic component of the incremental shear displacement and Δu_s is the total incremental shear displacement (Fig. 3).

Normal stiffness, shear stiffness, cohesion, friction and tensile strength can be assigned to the contacts. These properties are termed micro-properties in this work. Through an assembly of triangular blocks, the Trigon material represents a specific mechanical behavior which can be determined by the assumed macro-properties. Cracks initiate at a contact when the stress applied on the contact exceeds either its tensile strength or its shear strength. The Coulomb slip model is used in this work. The contacts may fail in either shear or tension according to the stress state (Gao et al. 2014b).

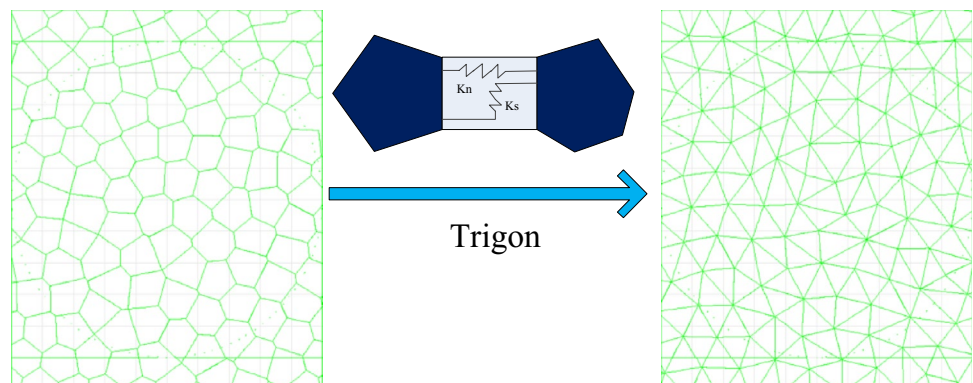
2.2 Modification of Rock Strata and RBB Parameters

The mechanical behavior of the material in the UDEC Trigon model is related to the micro-properties of contacts and blocks. The micro-properties must be calibrated to material properties. The generalized lithostratigraphy of the test site is illustrated in Fig. 4.

Indicators such as RQD, RMR, JCR and GSI are commonly used to evaluate rock qualities and classify rocks. Zhang and Einstein (2004) determined the relationship between RQD and ratio between the elastic modulus of the rock mass and the elastic modulus of the rock sample (Eq. 5).

$$\frac{E_m}{E_r} = 10^{0.0186RQD-1.91}, \tag{5}$$

Fig. 3 Illustration of the conventional UDEC model polygons transformed by Trigon logic for defining triangular finite difference zones



where E_m is the elastic modulus of the rock mass and E_r is the elastic modulus of the rock sample.

The uniaxial compressive strength of the rock mass can be determined by the functional relationship between the uniaxial strength ratio ($\bar{\sigma}_{cm}/\bar{\sigma}_c$) and the ratio between the elastic modulus of the rock mass and the elastic modulus of the rock (E_m/E_r), as shown in Eq. 6. The value of q in Eq. 6 is 0.63 (Gao et al. 2014c):

$$\frac{\bar{\sigma}_{cm}}{\bar{\sigma}_c} = \left(\frac{E_m}{E_r}\right)^q \tag{6}$$

The tensile strength of the coal mass and rock mass is calculated at 1/10 of the uniaxial strength. The modified rock mass parameters are listed in Table 1.

The parameters of polygon blocks and contact surfaces in the model were determined from previous research (Gao et al. 2014b) and are given in Table 2.

The UDEC Trigon model is adopted to simulate the uniaxial compression test using the modified rock mass parameters to verify the rationality of the micromechanical parameters of the coal mass and the rock mass. The size of the rock sample is 2 m (in width) × 4 m (in height) (Singh 2005) (Fig. 5). The bottom of the numerical model was fixed and a loading rate of 0.2 m/s was applied at the top. The test results are given in Table 3. The uniaxial compressive strength and

Fig. 4 Geological histogram

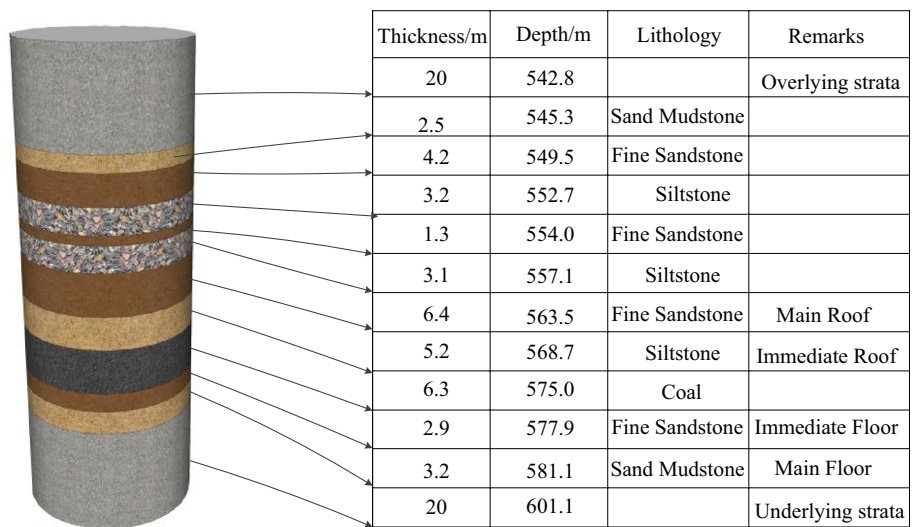


Table 1 Intact rock properties and scaled rock mass properties at Yuwu coal mine

Lithology	Intact rock		RQD (%)	Rock mass		
	E_r (GPa)	$\bar{\sigma}_r$ (MPa)		E_m (GPa)	$\bar{\sigma}_{cm}$ (MPa)	$\bar{\sigma}_{tm}$ (MPa)
Coal	2.6	11.2	65	0.52	2.3	0.23
Sandy mudstone	5.4	35.5	90	3.1	25	2.5
Fine sandstone	10.3	41.1	86	5.0	26.1	2.6
Siltstone	9.7	53.5	88	5.2	36.1	3.6

Table 2 Simulation parameters for various rock specimens used in the UDEC model

Lithology	Matrix properties		Contact properties				
	Density (kg m ⁻³)	E (Gpa)	k_n (GPa/m)	k_s (GPa/m)	Cohesion (MPa)	Friction (°)	Tensile strength (MPa)
Coal	1400	2.6	74.7	29.8	0.64	18	0.32
Sandy mudstone	1800	5.4	372	149	6.2	30	1.8
Fine sandstone	2650	10.3	639	236	8.7	18	1.8
Siltstone	2550	9.7	665	266	11.2	18	1.8

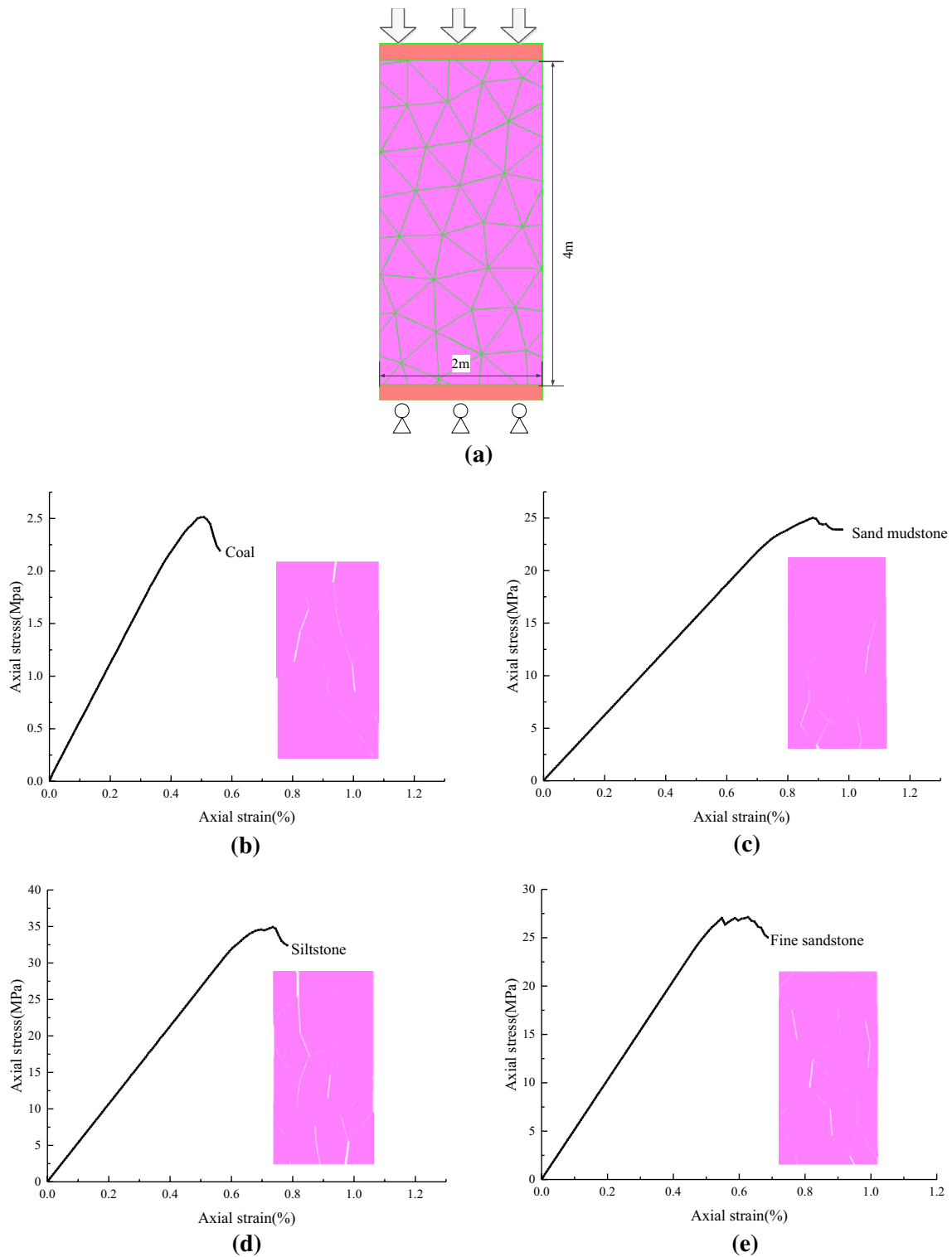


Fig. 5 Results of uniaxial compressive strength testing **a** numerical simulation of uniaxial compression, **b** stress–strain curve of coal, **c** stress–strain curve of sandy mudstone, **d** stress–strain curve of siltstone and **e** stress–strain curve of fine sandstone

elastic modulus data derived by numerical simulation are close in value to the data obtained from laboratory tests (within an error of 10%). Hence, the reasonable availability

of the micromechanical parameters of the coal mass and the rock mass is verified.

A uniaxial compression test is performed on the RBB sample. The strain-softening constitutive model is used to

verify the rationality of the mechanical parameters. The RBB has a water to cement ratio of 1.5:1. Comparison between the test results and the data obtained in the laboratory (Fig. 6a) suggest that the parameters selected in Table 4 are rational and can be used in further study of the RBB.

3 Evolution Mechanism and Parameter Optimization of Cracks in RBB

3.1 Mining and Geological Conditions

The Yuwu coal mine is located in Changzhi City, Shanxi Province, China. The geographical location of the mine and roadway layout of N2105 working face is given in Fig. 7.

The N2105 working face is in the #3 coal seam of Yuwu coal mine. The coal seam dips at 1.5° with a thickness of 6.4 m. The average overburden depth of the coal seam is 575 m. Stratigraphically, the immediate roof in the area consists of 5.2-m-thick siltstone with thick layering and

Table 3 Comparison between experimental and simulated values of Young’s modulus and peak stress for the various lithologies

Lithology	Young’s modulus (GPa)			Compressive strength(MPa)		
	Target	Calibrated	Error (%)	Target	Calibrated	Error (%)
Coal	0.52	0.51	2	2.3	2.54	10
Sandy mudstone	3.1	2.85	8	25	25	0
Fine sandstone	5	4.8	4	26.1	26.6	2
Siltstone	5.2	4.7	9	36.1	35	3

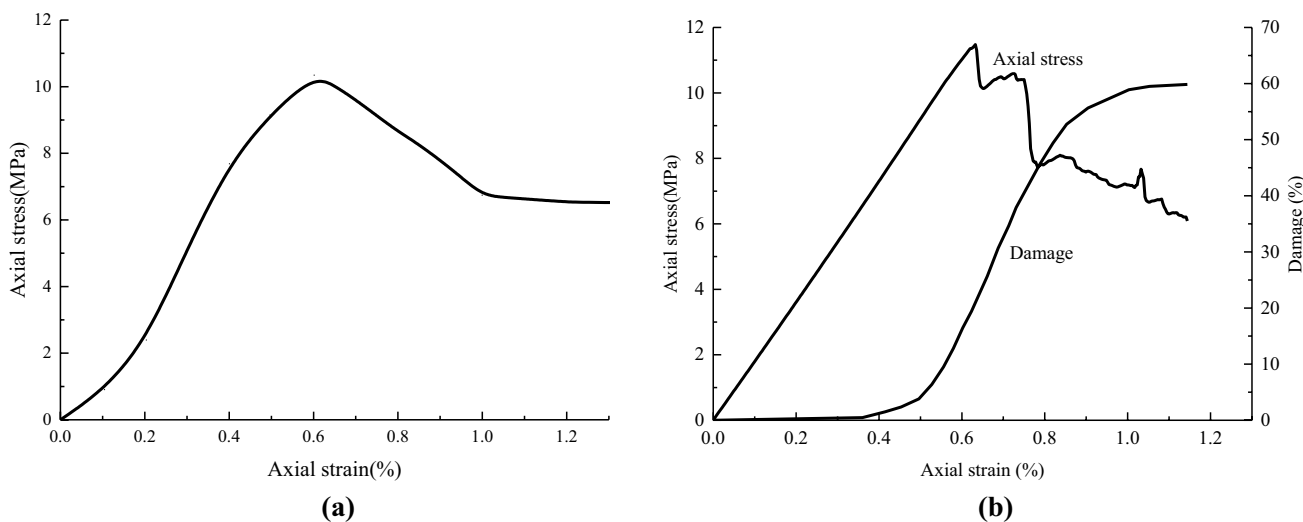


Fig. 6 Comparison between experimental and simulated results. **a** Experimental stress–strain curves of the RBB, **b** simulated stress–strain and damage curves of the RBB

Table 4 Mechanical parameters of blocks and joints of the RBB

	Density (kg/m ³)	Young’s modulus (GPa)	Cohesion (MPa)	Friction (°)	Tension (MPa)
Block	1400	0.15	3.8 ($\epsilon_p=0$) 3.3 ($\epsilon_p=0.06$) 2.7 ($\epsilon_p=0.2$)	33	2.3
Joint	Normal stiffness (GPa/m)	Tangential stiffness (GPa/m)	Cohesion (MPa)	Friction (°)	Tension (MPa)
	21.33	8.53	2.8	30	1.2

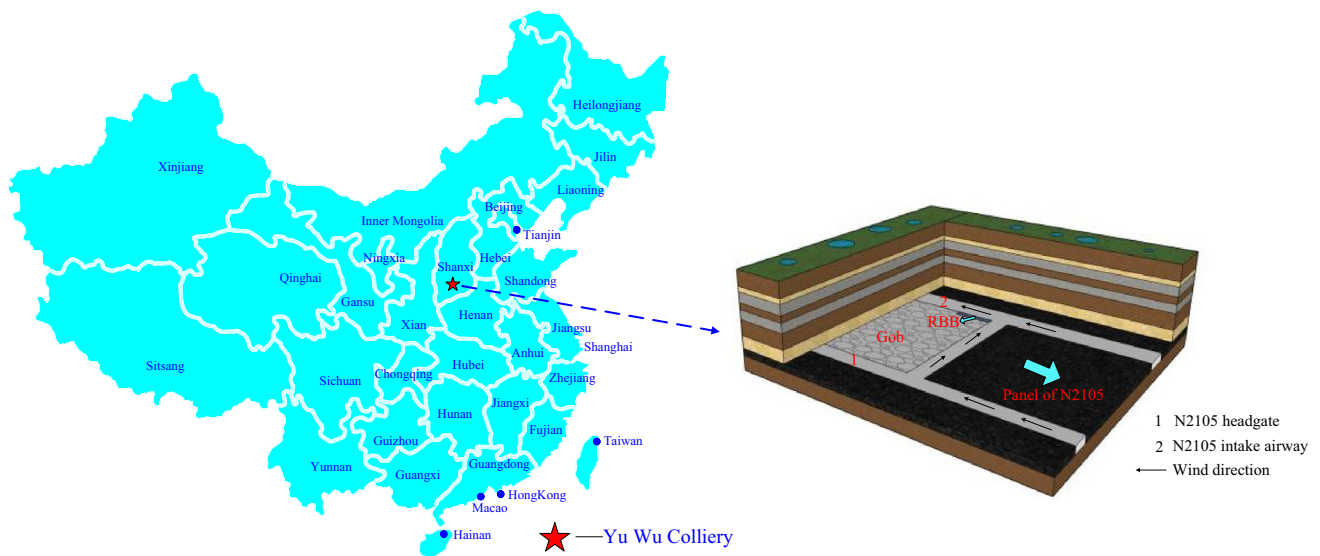


Fig. 7 Locality map of China showing the position of the Yuwu coal mine roadway layout of N2105 working face

uniform stratification. The main roof comprises 6.4-m-thick fine sandstone, also with thick layering and uniform stratification. The immediate floor is 2.9-m-thick fine sandstone, and the main floor is 3.2-m-thick sandy mudstone (Fig. 4). During the advance of the working face, gas emission aggravates the problem of gas gathering in the upper corner of the working face. The application of GER in the intake airway can effectively solve the ventilation problem. The Cross section of the N2105 panel is shown in Fig. 8.

3.2 Simulation Methodology

The UDEC Trigon model is used to simulate the N2105 intake airway GER in accordance with the geological conditions and to study the evolution of cracks in the RBB. The RBB, the other blocks and the contact surfaces in the model are simulated by the strain-softening model, elastic block model and the Coulomb slip model, respectively. The strain-softening model is based on the UDEC Mohr–Coulomb model with non-associated shear and associated tension flow rules. In this model, the user can define the cohesion, friction and dilation as piecewise linear functions of a hardening parameter that measures the plastic shear strain (Itasca Consulting Group Inc. 2014).

For computational efficiency, the UDEC Trigon approach is adopted to generate triangular blocks in the area of interest surrounding the roadway and RBB. The horizontal displacement is constrained at the left and right boundaries of the model. The vertical and horizontal displacements are fixed at the base. Regions (20 m in length) are preserved at the left and right sides of the model to avoid the boundary effect. Based on the depth of the longwall panel, the vertical stress applied on the upper boundary is 14.375 MPa with a stress gradient of 0.025 MPa/m. In this numerical model, the horizontal in situ stresses σ_H and σ_h are 13.066 MPa, where σ_H and σ_h are the stresses parallel and orthogonal to the longwall advance direction, respectively. The modeling processes are described as follows: (1) establish the model and assign the calibrated parameters of each rock formation; (2) calculate the initial state induced by gravity; (3) simultaneously excavate and support the N2105 intake entry; and (4) model retention of the N2105 intake entry with respect to different RBB aspect ratios (1:3.6, 1:1.8 and 1:1.2). Finally, the evolution processes of cracks in RBB at different aspect ratios are analyzed (Fig. 9).

Fig. 8 Cross section of the N2105 panel with RBB

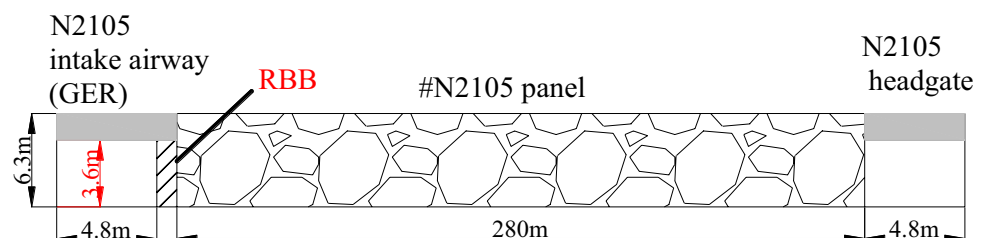
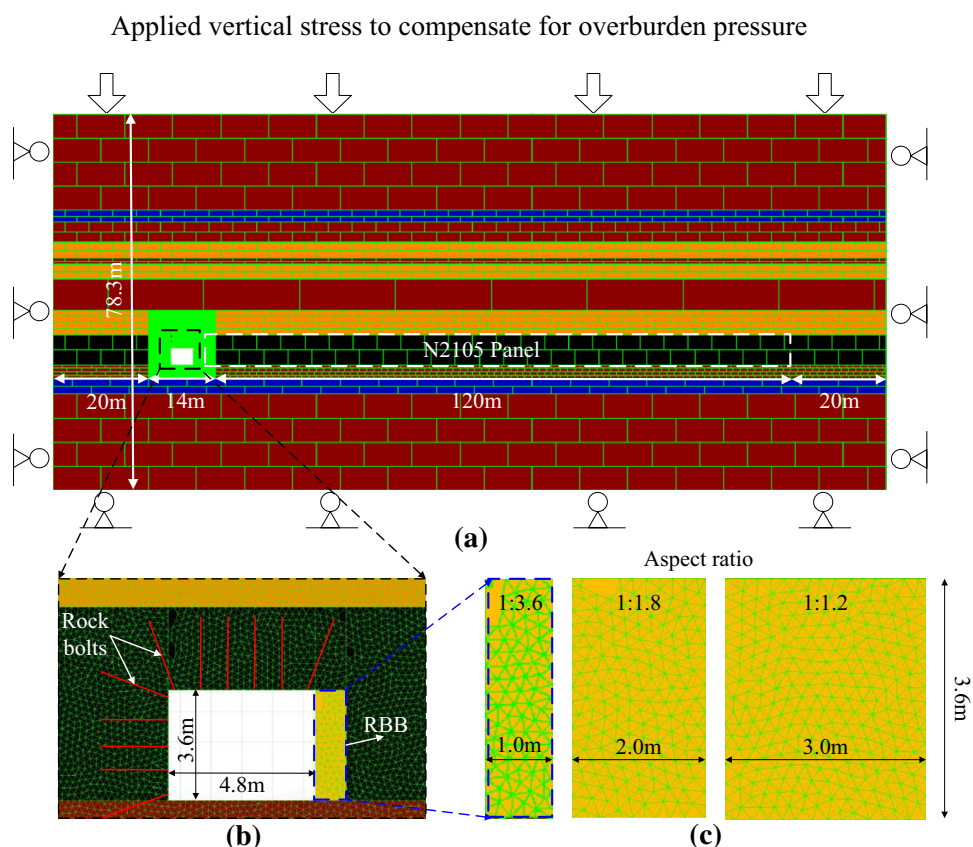


Fig. 9 Model overview. **a** Model dimensions; **b** dimensions of gob-side entry retaining structure; **c** aspect ratio of RBB



3.3 Evolution Mechanism of Cracks in the RBB with Aspect Ratio of 1:3.6

The evolution of RBB fracturing is studied in an RBB with an aspect ratio of 1:3.6. The RBB is completely destroyed after the advance of the working face (Fig. 10).

Due to the difficulty of determining the RBB strain in the numerical model, the crack evolution processes of the RBB are studied in this work based on the stresses, cracks and damage degree at different distances from the working surface. The FISH language is used to monitor the number and the length of shear cracks and tensile cracks in the RBB to further study the damage mechanism of the RBB. Figure 12 presents the monitoring results. The damage degree of the RBB is determined by the ratio of damage length of the contact surface (including both shear cracks and tensile cracks) to the total length (Gao et al. 2014a). This method is used in this work instead of the “orthogonal strain ratio” commonly used in previous studies because of the intractability of the strain of the RBB in the numerical simulation (i.e., the ratio of transverse strain to the axial strain of the rock mass).

Figure 10 shows the damage of RBB and surrounding rocks before and after excavation of the working face. Figure 11 illustrates the crack development and failure of RBB at different distances from the working face. It gives the formation, expansion and penetration of cracks, as well as

the whole process of macro-fracturing of the RBB. When the RBB is located at -10 m, the RBB is destroyed due to the formation of main cracks in its middle and bottom parts. When the RBB is located at -40 m, significant shear failure is found in the upper left corner of the RBB. Also, two smaller cracks develop at the right side of the main crack with tensile damage distributed around the main crack. Significant tensile failure is observed in the bottom of the RBB when it is located at -80 m. Meanwhile, a seepage channel appears in the damaged RBB, resulting in the loss of the buffering function of the RBB.

It is commonly recognized that two stress thresholds of the rock exist before the stress reaches the peak strength, including the crack initiation threshold and the crack damage threshold. There is some controversy about the definition of these two values, one of which is that both of these values can be determined by acoustic emission and strain monitoring (Eberhardt 1998). The other is that the crack initiation threshold is indicated by the occurrence of simulated discrete cracks and the crack damage threshold can be identified by acceleration in the crack accumulation rate (Diederichs 1999). In this paper, the timing of the two values, the corresponding mechanical parameters of the RBB and the damage parameters are studied. The growth of shear cracks becomes stable and the growth of tensile cracks is drastic once the stress in the RBB reaches the crack damage threshold, and

Fig. 10 Surrounding rock conditions **a** before and **b** after mining. Note the ingress of gas along preferential flow channels

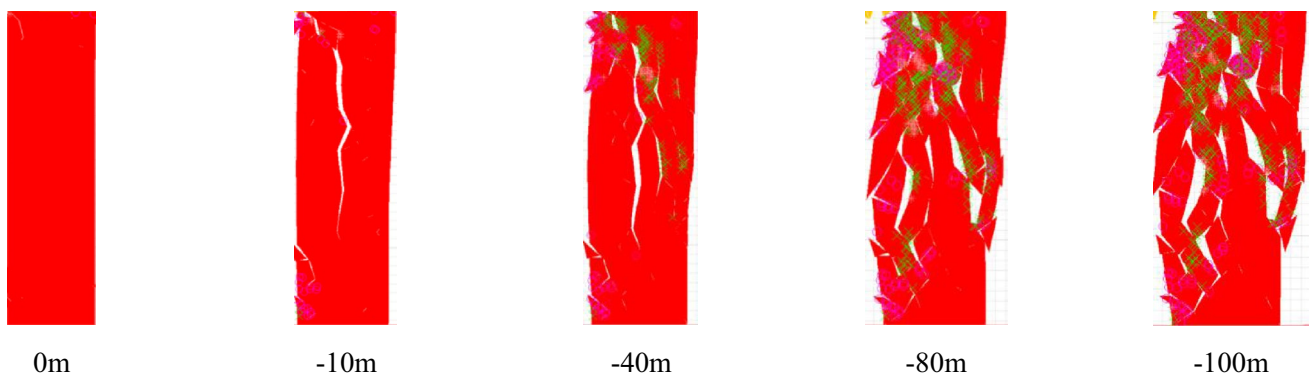
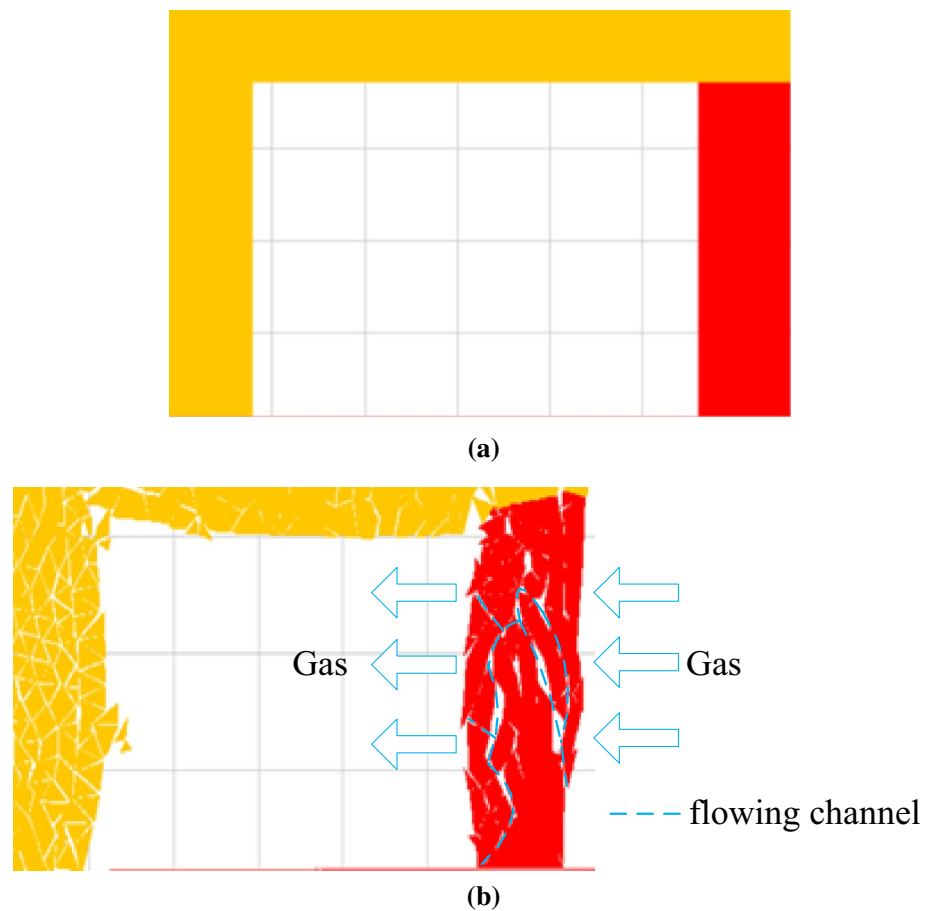


Fig. 11 Progressive destruction process of the RBB from 0 to 100 m behind the working face (– indicates the RBB is located behind the work face; *at yield; circle: tensile failure; cross: yielded in past)

obvious cracks appear in the RBB after the crack damage threshold was reached.

The strength of the RBB is 10.6 MPa (Fig. 12a). The stress value at the onset of cracking in the RBB is 16% of the peak stress (i.e., the crack generation threshold). When the RBB is located at –40 m, and the applied stress value reaches 72% of the peak stress, the inflection point of the RBB damage curve appears. It can be considered that the

crack damage threshold is reached at this time, and the obvious damage is found in RBB. Based on the damage map of the RBB at –40 m in Fig. 11, it is believed that the damages in the upper left and lower left corners of the RBB are mainly caused by shear and tensile cracking. Shear cracks predominate in quantity throughout the crack evolution. The tensile cracks and failures in Fig. 12b, c are enlarged to investigate the development of tensile cracks (Fig. 12d).

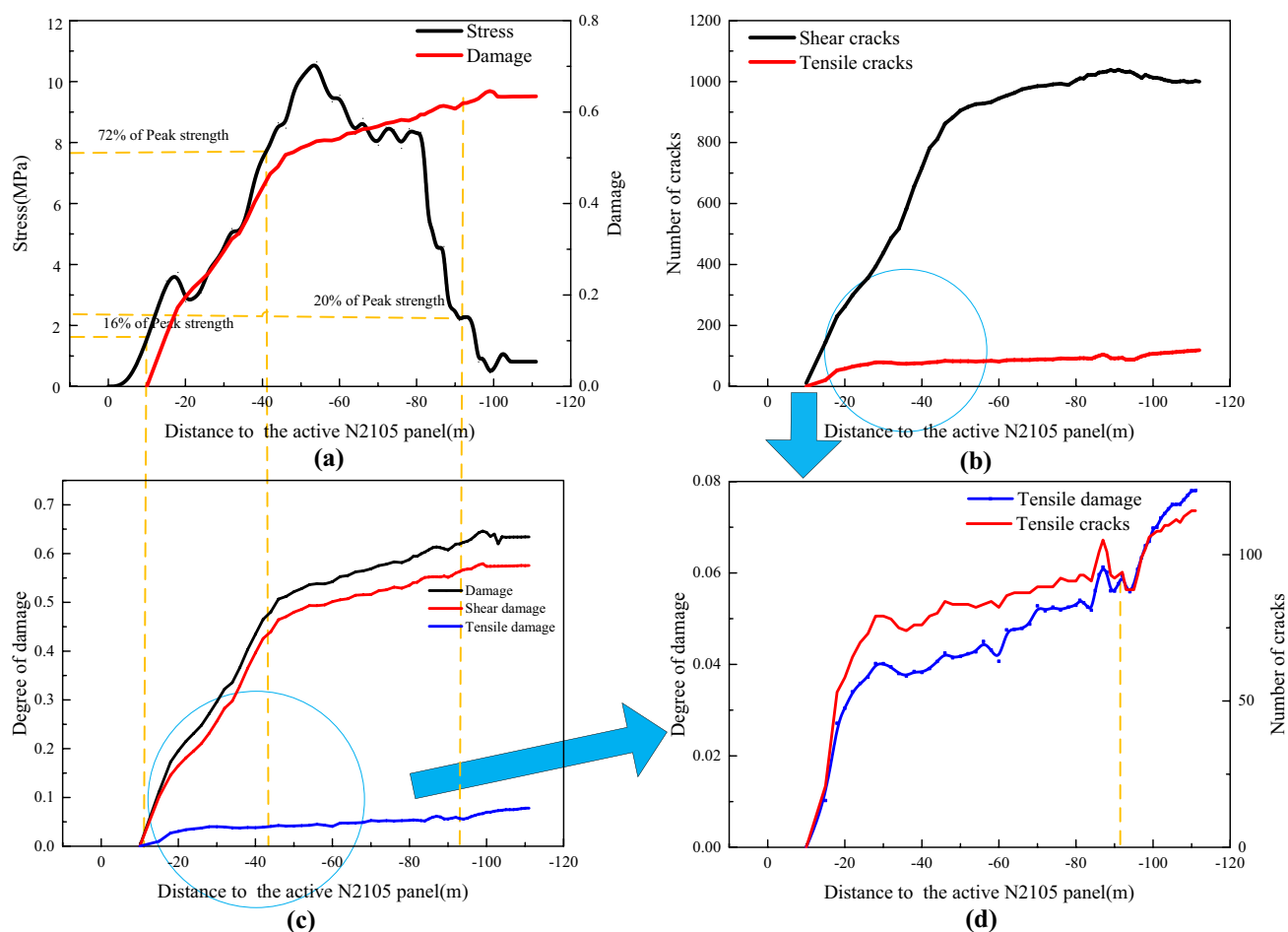


Fig. 12 UDEC Trigon simulation results showing **a** stress and damage evolution, **b** increase in cracks, **c** and **d** increase in damage during excavation of the N2105 working face

In comparison with Fig. 11, it is found that the number of tensile cracks and the degree of tensile failure are all in an ascending tendency before visible failure of the RBB occurs at -40 m. Obvious crack development and dilation are found in the RBB 40 m behind the working face (Fig. 11). The stress in the RBB 90 m behind the working face drops to 20% of its peak strength with the RBB being seriously damaged. Development of shear cracks in the RBB tends to become steady at this time, while tensile cracks continue to develop (Fig. 12d). Hence, the generation, expansion and penetration of tensile cracks are the dominant factors leading to failure of the RBB, although the shear cracks predominate in quantity during the whole process of crack evolution in the RBB.

3.4 Optimization design of RBB parameters

One purpose of this work is to simulate the RBB at different aspect ratios (1:1.8, 1:1.2). Then the stress and the damage are monitored to determine the most suitable parameters of

the RBB for the N2105 intake airway. The damaged RBB and damage area division are shown in Fig. 13.

The RBBs at aspect ratios of 1:1.8 and 1:1.2 suffer significantly less damage compared with the RBB at an aspect ratio of 1:3.6 (Fig. 13). Moreover, there is no penetration of cracks into the RBB. This prevents the formation of a gas exchange channel. Figure 13a, c indicates that the damage in the RBB is mainly concentrated on the surface and shallow regions. The damaged RBB can be divided into three zones based on crack distribution and damage degree in different areas in the interior of the RBB. They include the main crack-development zone (zone A), the yield-bearing zone (zone B) and the secondary crack-development zone (zone C). The damage degree is 60% when the RBB sample reaches the residual strength (Fig. 6b). Therefore, it is concluded that the RBB loses the bearing capacity when the damage degree exceeds 60%. (Gao et al. 2014a, b). In the model, the damage degree is monitored for each area in the RBB at different aspect ratios. The results in Fig. 14 suggest that the damage degree of zone B is lower

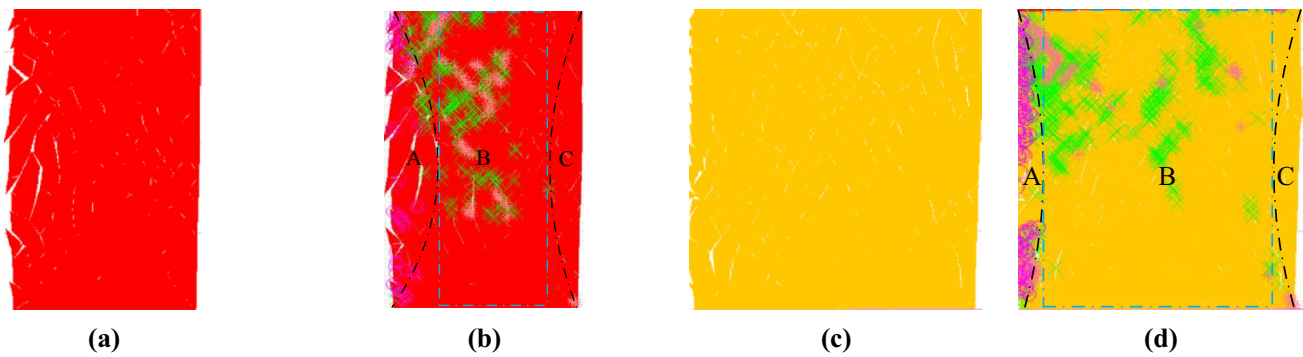


Fig. 13 Damaged RBB and damage area division showing **a** RBB with aspect ratio of 1:1.8, **b** RBB area division with aspect ratio of 1:1.8, **c** RBB with aspect ratio of 1:1.6 and **d** RBB area division with aspect ratio of 1:1.6 (*at yield surface; circle: tensile failure; cross: yielded in past)

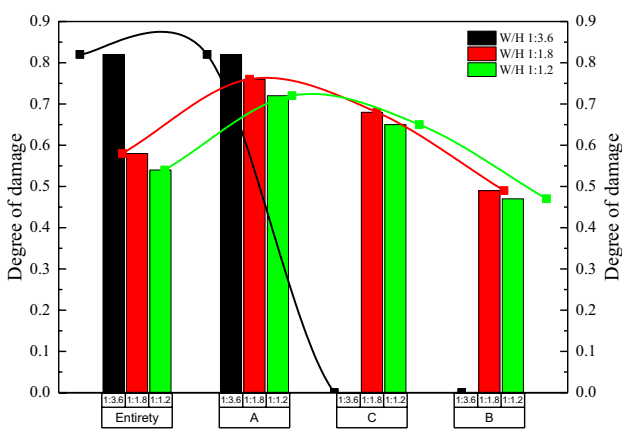


Fig. 14 Histograms showing comparisons of damage for different aspect ratios of the RBB

than 50%, whereas the damage degree of zone A and zone C is greater than 60%. In this case, the zone A and zone C are considered to lose load-bearing capacity. Fewer tensile cracks are found in zone C compared with that in zone A. Also, no obvious tensile damage is observed in zone C. The main crack-development areas are the most damaged parts of the RBB and are distributed at the top and bottom corners of the roadway (Fig. 13b, d). The main form of damage in these areas is tensile failure. The development of cracks in the secondary crack-development zone is relatively low, and there is only a small amount of tensile failure in the bottom corner of the RBB. The RBB in the yield-bearing zone is basically in a yield or elastic state, with a low damage degree. The area of the yield-bearing zone in the RBB at aspect ratios of 1:1.8 and 1:1.2 account for 51% and 82%, respectively (Fig. 13b, d).

Figure 14 compares the damage degree of the RBB at different aspect ratios (1:3.6, 1:1.8 and 1:1.2). The overall damage, damage degree in the main crack-development area, damage degree in the secondary crack-development

zone and damage degree in yield-bearing zone are compared in the following text.

The whole part of the RBB with an aspect ratio of 1:3.6 is classified as a main crack-development zone due to high damage degree in the highly fractured RBB with this aspect ratio. The histograms in Fig. 14 indicate that the overall damage and damage different zones decrease with an increasing aspect ratio. The damage degree in the main crack-development zone is the highest, while the damage degree in the yield-bearing zone is the lowest. The damage degree in the yield-bearing area of the RBB at an aspect ratio of 1:1.8 is 49%, and damage degree in the yield-bearing zone of the RBB at an aspect ratio of 1:1.2 is 47%.

The above results suggest that the yield-bearing zone of the RBB at an aspect ratio of 1:1.8 is much higher than that at an aspect ratio of 1:1.2. However, the damage degree in the yield-bearing zone has a reduction of only 2%. The larger proportion of the yield-bearing area does not effectively reduce the damage degree of the RBB, although the larger RBB width occupies coal resources and has an impact on the economic efficiency of the coal mine. Therefore, the width of the RBB at the working face is set to 2 m (i.e., an RBB with an aspect ratio of 1:1.8).

It is shown that an RBB with an aspect ratio of 1:1.8 can basically meet the safe mining requirement, but the surface and shallow parts close to the roadway side of the RBB are severely damaged. This can easily lead to rib spalling. Therefore, counter-pulled bolts are used to reinforce the RBB. It can be verified by numerical simulation that the counter-pulled bolts have a notable effect on damage development in the shallow region of the RBB. Hence, potential rib spalling can be prevented. Meanwhile, multi-factor analysis is performed to study the total damage degree, the area ratio of the yield area, the residual strength of the yield area, the peak stress position of the yield area and the peak stress magnitude in the yield area for RBBs at different sizes. The results are presented in Fig. 15. An aspect ratio of 1:1.8 leads to a certain reduction of the main and

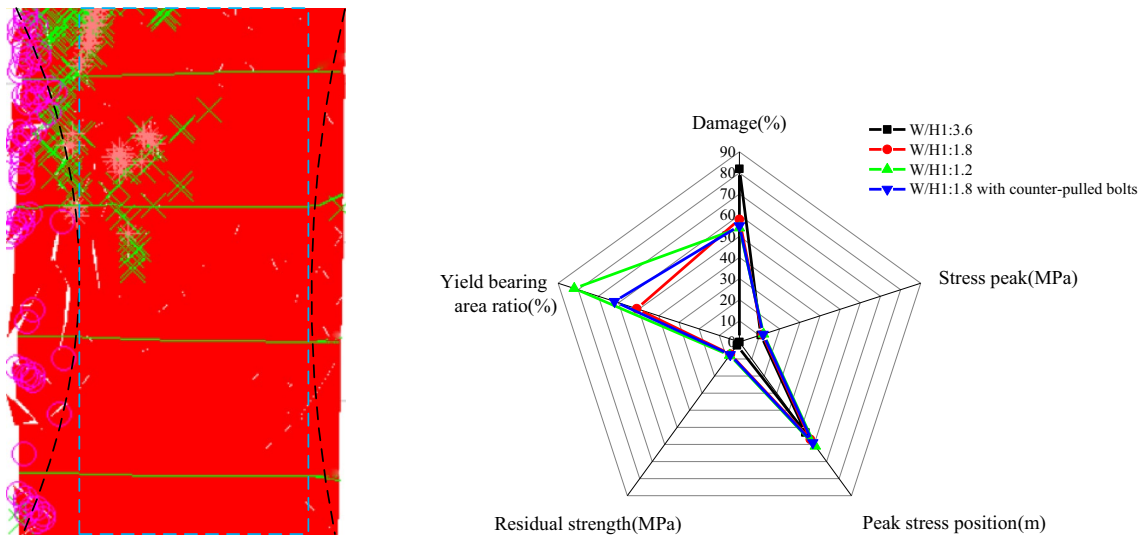


Fig. 15 Multivariate analysis of the RBB for different aspect ratios

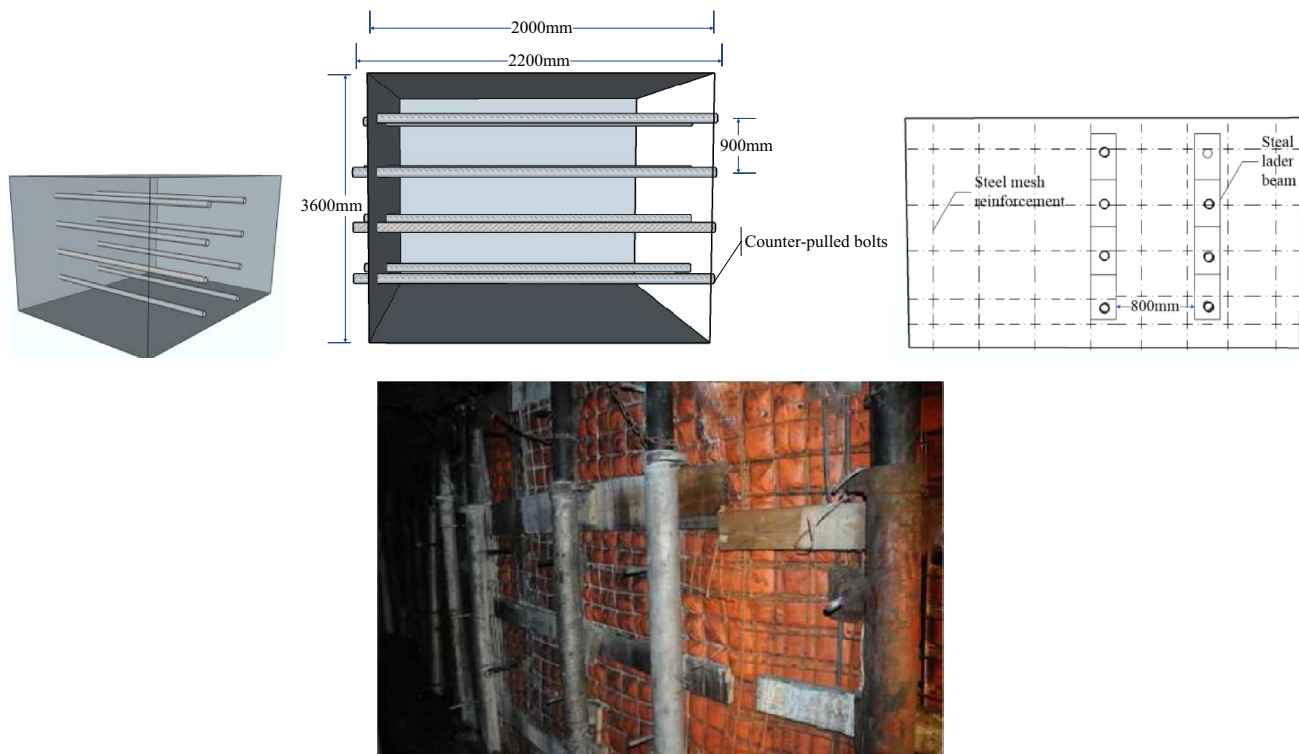


Fig. 16 Schematic diagrams and photograph of road-side support

secondary crack-development areas after reinforcement with counter-pulled bolts and a significant reduction of vertical cracks with large apertures at the roadway side. The damage degree in the yield-bearing zone is 55%. The peak stress in the yield-bearing zone reaches 11.8 MPa, appearing 59 m behind the working face. The residual strength of the yield

area is 7.4 MPa and the proportion of the yield-bearing zone is 62%.

From the above analysis, it is concluded that all indicators of damage to the RBB at an aspect ratio of 1:1.8 (Fig. 15) are enhanced after reinforcement with the counter-pulled bolts. Insufficient surface maintenance of the RBB can also

be strengthened by laying a metal mesh over the surface of the RBB.

4 Field Tests and Observations

4.1 Field Test Results

The technology of GER is applied to the intake airway of N2105 working face to decrease unacceptable high gas density. The tunnel section size is 4800 mm × 3600 mm. The support parameters are given as follows:

Road-in support parameters: The roof and side are both supported by high strength bolts with dimensions of 22 mm × 2200 mm. The roof is supported with anchors 18.9 mm × 8300 mm in dimension. The inter-row spacing of the roof bolts is 900 mm × 880 mm, while the inter-row spacing of bolts in the solid coal body is 900 mm × 800 mm. The anchor cable rows are to be spaced at 1600 mm along the length of the entry. The pretension for the rock bolt and anchor cable installation are 200 kN and 510 kN, respectively.

Roadside support parameters: The RBB is constructed by a relatively high-water content material, with a water–cement ratio of 1.5:1. The aspect ratio of the RBB is 1:1.8, and a metal mesh was installed on the surface of the RBB. Counter-pulled bolts (22 mm in diameter and 2200 mm in length) are used. The inter-row spacing of the counter-pulled bolts is 900 mm × 800 mm, and a reinforcing steel ladder beam (Φ16 mm steel bar) is added for reinforcement (Fig. 16).

4.2 Observations

Retention of the intake airway is monitored during advance of N2105 working face to analyze the efficiency of GER. The following parameters are monitored: deformation of roadway surrounding rocks, bearing capacity of the RBB and gas concentration in the roadway and upper corner (Fig. 17).

When the working face advances to the station, the internal stress of the station increases gradually and reaches a peak of 9.5 MPa at a distance of 53 m ahead of the working face. The stress decreases gradually in the RBB 53 to 100 m behind the working face. The stress becomes steady (7.8 MPa) in the RBB 100 m behind the working face and remains stable with the advance of the working face. Deformation of the roadway surrounding rocks increases gradually with advance of the working face. The entry section 100 m in front of the station is stable. The maximum roof-to-floor convergence is 527 mm, while the maximum rib-to-rib convergence is 515 mm. From gas monitoring results, the gas densities in the upper corner and in the roadway are 0.5%

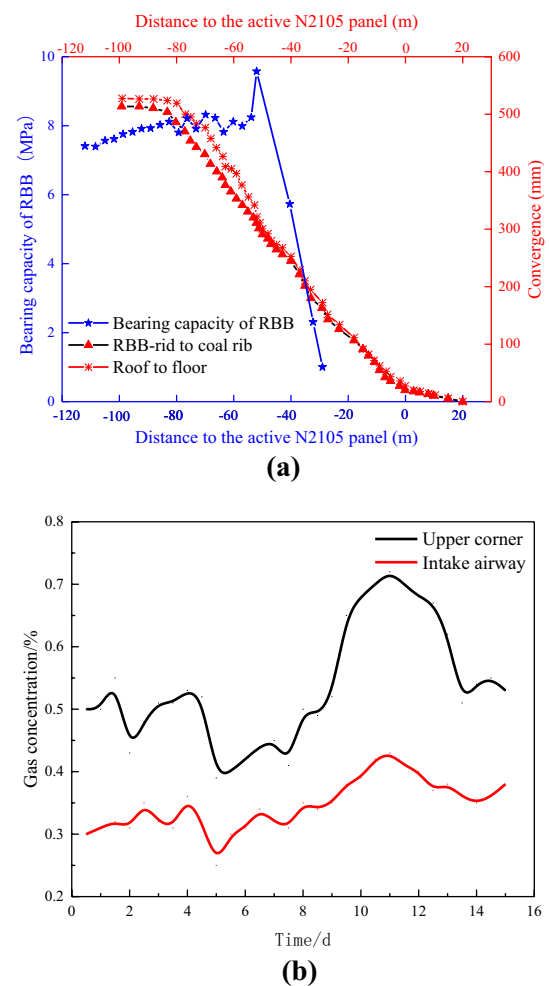


Fig. 17 N2105 monitoring results during mining showing **a** convergence of GER and the bearing capacity of the RBB **b** changes in gas concentration over time

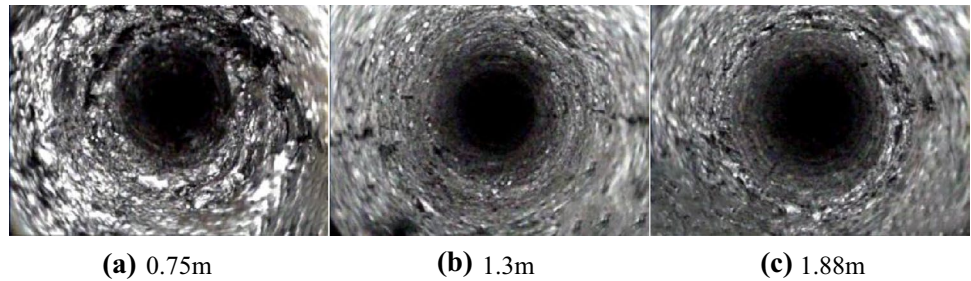
and 0.35%, respectively. These values are in the safe density range.

Figure 18 gives three screenshots from video footage recorded at depths of 0.75 m, 1.3 m and 1.88 m in the RBB at a distance of 100 m behind the working face. It is shown that the development of cracks in the road side that the middle part of the RBB are essentially consistent with the simulation, which verifies the rationality of the choice of aspect ratio of the RBB and roadway support parameters.

5 Conclusions and Expectation

GER has been widely used in China's coal mines due to its high recovery rate and low drivage ratio. Field test and numerical simulation are utilized to investigate the crack evolution in the RBB optimizing the RBB aspect ratio. The main results of this study are summarized as follows.

Fig. 18 Screenshots taken from video obtained down boreholes in the RBB at **a** 0.75 m depth, **b** 1.3 m depth and **c** 1.88 m depth



1. A UDEC Trigon model is adopted to simulate the crack evolution in the RBB. The input parameters are calibrated. The simulated results are consistent with those from laboratory experiment. The damage-bearing relationship of RBB is defined according to the stress and damage curve of RBB specimen obtained from numerical simulation. When the damage degree of RBB reaches greater than 60% and the stress is lower than the residual strength, the RBB is considered to have no bearing capacity.
2. The initiation, propagation and coalescence of internal cracks are investigated throughout the N2105 longwall mining. The crack initiation threshold occurs at about 16% of the peak strength and the crack damage threshold occurs at about 72% of the peak strength. Failure of the RBB is mainly caused by tensile cracks, although shear cracks are dominant in number during the whole process of crack development of the RBB. According to the crack distribution and damage degree, the damaged RBB is divided into three zones (i.e., the main fissure development zone A, the yield-bearing zone B and the secondary crack-development zone C). Higher aspect ratio and using counter-pulled bolts could effectively increase the area proportion of zone B and reduce the damage degree of zone B.
3. According to this mechanism of crack evolution, an optimal RBB aspect ratio is proposed and support measures are recommended to implement in the intake airway of the N2105 coal face. Field applications show that the resulting roof-to-floor and rib-to-rib convergence are 527 mm and 515 mm, respectively. These support recommendations provide a basis for the planning and design of RBB under similar engineering and geological conditions.

Effective use of underground spaces, such as underground storage of hydrogen or nuclear waste, has significance for saving land resources. Such gas or nuclear waste reservoirs must have reliable cover to prevent vertical leakage and overall tightness to prevent lateral leakage. As such, it is anticipated that the research method presented here can be used to detect gas–liquid permeability when the wall is closed to ensure adequate sealing of the storage space.

Acknowledgements The authors are grateful for the support from “The Fundamental Research Funds for the Central Universities (2017XKZD06)”.

References

- Alzo'ubi AM (2009) The effect of tensile strength on the stability of rock slopes. Ph.D. thesis, University of Alberta
- Bi JG (2014) Study on stability of surrounding rock and roadside backfill body of gob roadway driven by fully mechanized caving face. Master thesis, Taiyuan University of Science and Technology
- Chen Y (2012a) Study on stability mechanism and control of surrounding rock structure along goaf roadway. Ph.D. thesis, China University of Mining and Technology
- Chen Y, Bai JB, Zhu TL et al (2012b) Mechanisms of roadside support in gob-side entry retaining and its application. *Rock Soil Mech* 33(5):1427–1432. <https://doi.org/10.3969/j.issn.1000-7598.2012.05.023>
- Christianson M, Board M, Rigby D (2006) UDEC simulation of triaxial testing of lithophysal tuffs. In: Proceedings of the 41st U.S. rock mechanics symposium, paper ARMA-06-968
- Diederichs MS (1999) Instability of hard rock masses: the role of tensile damage and relaxation. Ph.D. thesis, University of Waterloo
- Eberhardt E (1998) Brittle rock fracture, progressive damage in unconfined compression. Ph.D. thesis, University of Saskatchewan
- Gao FQ, Stead D, Coggan J (2014a) Evaluation of coal longwall caving characteristics using an innovative udec trigon approach. *Comput Geotech* 55(5):448–460. <https://doi.org/10.1016/j.compgeo.2013.09.020>
- Gao FQ, Stead D (2014b) The application of a modified voronoi logic to brittle fracture modelling at the laboratory and field scale. *Int J Rock Mech Min Sci* 68(68):1–14. <https://doi.org/10.1016/j.ijrmm.2014.02.003>
- Gao FQ, Stead D, Kang H et al (2014c) Discrete element modelling of deformation and damage of a roadway driven along an unstable goaf—a case study. *Int J Coal Geol* 127(7):100–110. <https://doi.org/10.1016/j.coal.2014.02.010>
- Guo JJ (2017) Study on crack evolution and permeability change mechanism of medium and high rank coal in the process of bearing stress. Ph.D. thesis, Southwest Petroleum University
- Hao SP (2017) Study on stability mechanism of backfill body in gob-side entry retaining. Master's thesis, China University of Mining and Technology
- Itasca Consulting Group Inc (2011) UDEC (Universal Distinct Element Code), Version 4.1. Itasca, Minneapolis
- Itasca Consulting Group Inc (2014) UDEC (Universal Distinct Element Code), Version 6.0. Itasca, Minneapolis
- Kan JG, Zhang N (2011) Analysis of supporting resistance of backfilling wall for gob-side entry retaining under typical roof conditions. *Rock Soil Mech* 32(9):2778–2784. <https://doi.org/10.3969/j.issn.1000-7598.2011.09.036>

- Khaldoun A, Ouadif L, Baba K et al (2016) Valorization of mining waste and tailings through paste backfilling solution, imiter operation, morocco. *Int J Min Sci Technol* 26(3):511–516. <https://doi.org/10.1016/j.ijmst.2016.02.021>
- Li YF, Hua XZ (2012) Mechanical analysis of stability of key blocks of overlying strata for gob-side entry retaining and calculating width of roadside backfill. *Rock Soil Mech* 33(4), 1134–1140. <https://doi.org/10.16285/j.rsm.2012.04.027>
- Li GD, Wang XY (2017) Study of numerical simulation and control technology of fracture characteristics of gob rock in gob roadway. *J Coal Sci Technol* 45(4):50–55
- Li X, Ju M, Yao Q et al (2016) Numerical investigation of the effect of the location of critical rock block fracture on crack evolution in a gob-side backfill wall. *Rock Mech Rock Eng* 49(3):1041–1058. <https://doi.org/10.1007/s00603-015-0783-1>
- Lisjak A, Grasselli G (2014) A review of discrete modeling techniques for fracturing processes in discontinuous rock masses. *J Rock Mech Geotech Eng* 6(4):301–314. <https://doi.org/10.1016/j.jrmge.2013.12.007>
- Lorig LJ, Cundall PA (1989) Modeling of reinforced concrete using the distinct element method. *Fracture of concrete and rock*. Springer, New York
- Ma LQ, Zhang DS, Chen T (2007) Study on packing body supporting resistance of enter-in packing for in-situ gob-side entry retaining in fully mechanized top-coal caving mining face. *J Rock Mech Eng* 26(3):544–550
- Ning J, Wang J, Bu T et al (2017) An innovative support structure for gob-side entry retention in steep coal seam mining. *Minerals*. <https://doi.org/10.3390/min7050075>
- Singh M, Rao KS (2005) Empirical methods to estimate the strength of jointed rock masses. *Eng Geol* 77(1–2):127–137. <https://doi.org/10.1016/j.enggeo.2004.09.001>
- Tan YL, Yu FH, Ning JG et al (2015) Design and construction of entry retaining wall along a gob side under hard roof stratum. *Int J Rock Mech Min Sci* 77:115–121. <https://doi.org/10.1016/j.ijrmms.2015.03.025>
- Xu WB, Wan CB, Tian XC (2018) Coupling effect of temperature and fracture on the strength and crack propagation mode of backfill mass. *J Min Saf Eng* 35(3):612–619. <https://doi.org/10.13545/j.cnki.jmse.2018.03.023>
- Zhang L, Einstein HH (2004) Using RQD to estimate the deformation modulus of rock masses. *Int J Rock Mech Min Sci* 41(2):337–341. [https://doi.org/10.1016/S1365-1609\(03\)00100-X](https://doi.org/10.1016/S1365-1609(03)00100-X)
- Zhang DS, Miao HX, Feng GM (2003) Testing study on deformation features of surrounding rocks of gob-side entry retaining in fully-mechanized coal face with top-coal caving Chinese. *J Rock Mech Eng* 32(3):232–235

Publisher's Note Springer Nature remains neutral with regard to jurisdictional claims in published maps and institutional affiliations.